

# Bio-inspired Amphibious Origami Robot with Body Sensing for Multimodal Locomotion

Huixu Dong<sup>\*1</sup>, Haitao Yang<sup>\*2</sup>, Shuo Ding<sup>\*1</sup>, Tong Li<sup>1</sup>, Haoyong Yu<sup>\*1</sup>

**Abstract**— Animals have long captured the inspirations of researchers in robotics with their unrivaled capabilities of multimodal locomotion on land and in water, achieved by functionally versatile limbs. Conventional soft robots show infinite degrees-of-freedom (DOFs), making it hard to be actuated and conduct multiple movements especially for multimodal locomotion in different environments. An origami robot, which is capable of reversibly transforming the robotic shape by simple creases folding/unfolding, reveals advantages for imitating flexible movements of animals, thus drawing more and more attention. However, it poses substantial technological challenges for bio-inspired design, sensing, and actuation of origami robots that can generate multimodal locomotion via performing complex morphologic deformation in different scenarios such as land and water. To relieve this issue, we propose a novel bio-inspired amphibious origami machine with body sensing for multimodal locomotion. In this work, inspired by the peristalsis of inchworm and human swimming behaviors, a unique origami body with legs and origami arms is developed to enable the integrated robot to move both on land and in water. Instead of traditional electronic sensors, we design highly stretchable and foldable layer resistive sensor with conductive polymers coated onto the origami body to achieve robotic sensing such as obstacle detection. In addition, with detailed analysis, a self-designed pneumatic system of time division, multiplexing, and serialization is adopted to efficiently control the robot with high-DOF. We eventually demonstrate that the fabricated origami robot successfully moves in amphibious environments, which is capable of crawling forward, turning right/left, and swimming. We expect this work indicates contributions to advanced origami design, actuation control, body sensor of the bio-inspired robot with multimodal locomotion for broadly practical applications.

**Index Terms**— Bio-inspired origami, Amphibious robot, Multimodal locomotion, Robotic sensing.

## 1. Introduction

Hundreds of thousands of years of species evolution create the current prosperity, where each creature demonstrates a unique organism to adapt to the changing world. As the masterpieces of nature, bionic functions have always been pursued in designing soft machines such as the water strider robot, inchworm robot, snack-mimicking robot, and so on[1-3]. In particular, several animal species like crabs and frogs demonstrate remarkable locomotive capabilities both on land and in water, which inspires the design of amphibious soft robots with varied locomotion modalities to adapt to mutative tasks[4, 5].

Indeed, the key of the amphibious soft robot is designing dynamic three-dimensional(3D) geometric structures which are reconfigurable to realize efficient multi-modal locomotion whether on land or in water. There exist research works regarding the structure design and actuation methods of amphibious soft robots. Researchers have studied the driving mechanism of organisms in different environments and then imitated their shapes and motion structures to design biomimetic robots[6, 7]. Recently, some control strategies based on switchable adhesion actuator, fluidic elastomer actuator, pneumatic artificial muscles, and shape memory alloys that are capable of motions have been exploited in bionic amphibious robots for multimodal locomotion [8-11]. However, it is challenging for conventional soft robots to be controlled and further perform various movements, especially for multimodal locomotion due to the infinite degrees-of-freedom (DOFs), which limits their practical applications[12]. In addition to locomotion, robotic sensing is also an important capability for soft machines, which is potentially used in the close-loop feedback control[13, 14]. Conventionally, people adopt extra electronic modules on robots. However, the equipment of additional modules would increase the overall weight of integrated robots, which contradicts the ultimate goals of creating light, compliant, and power-efficient robots with multifunctionality[15]. Alternatively, there are some reports adopting ultra-thin robotic skins, which enabled soft robots with various sensing capabilities with ignorable weight increase[16, 17].

Recently, origami structure, which is created from a sequence of programmable creases, provides a simple approach to reversibly transforming an object's shape/size and attracts more and more attention in developing soft machines[12, 18, 19]. Considering that the number of creases folding/unfolding is user-specified and governed by simple physical rules, origami structures show unique advantages in designing high-DOF soft robots with well-controlled multimodal locomotion, as well as the merits of lightweight and low-cost aspects. Nevertheless, there is a rare report for origami robots with amphibious locomotion and sensing capabilities. We expect the challenges lie in three main aspects. First, the principles of robotic locomotion on land and in water are totally different, which increases the difficulty in designing multiple origamis coordinated in one integrated robot that is capable of highly varied morphologies. Second, conventional robotic skins are hard to be tightly integrated onto origami robots due to their very irregular origami exoskeletons. A new integration strategy is desired for origami robots with body sensing. Third, there is a challenge for actuating an origami robot with high-DOF to realize variously morphological deformations.

Here, we present a novel bio-inspired amphibious origami robot with body sensing for multimodal locomotion. In this

<sup>1</sup>Bio-Robotics Lab, Department of Biomedical Engineering, National University of Singapore, Singapore 117583, Singapore; <sup>2</sup>Department of Chemical and Biomolecular Engineering, National University of Singapore, Singapore 117585, Singapore.

\*These authors contributed equally to this work.

†Corresponding author. Email: bieyhy@nus.edu.sg

study, taking imagination from inchworm and human swimming, we suggest a multi-modular origami robot that can perform impressive movement characteristics for various locomotion gaits. Those locomotion gaits are well simulated, analyzed, and thereafter are well controlled with a self-designed pneumatic system. Moreover, instead of equipping extra modules or attaching robotic skins, the alternative pathway is to create a functional robotic backbone with desired sensing capability. In particular, by coating conductive polymers on body origamis, built-in strain sensing is realized during robotic actuation, and we show its potential for obstacle detection. We demonstrate that our developed origami robot makes crawling, turning, and swimming motions on land and in water scenarios correspondingly (see Fig.1, the figure caption is listed on the last page).

## 2. Results

### A. Overall strategy

The crawling locomotion of the proposed robot attributes to the transformation of origami structure. That is, the origami deformation generates the robotic motion. As shown in Fig.2, the proposed crawling mechanism combines the octagon-origami structures, where the feet of the front and rear legs have different friction surfaces. The advantage of such a design is that, with the deformation of octagon-origami, it generates the alternating motions for the front and rear legs thus enabling the robotic body to realize multiple inchworm-like movements such as crawling forward, turning right, and turning left.

We configure multiple origami twisted towers and deploy the towers axes in a 3D space, which serves as the robot shoulder and allows the robot to perform complex human-like swimming motions (see Fig.1 and Fig.3). In particular, the robotic shoulder can rotate the arm to perform the forward and backward movements in water, imitating human swimming behaviors. It is worthy to note that, to realize the swimming motion, a thin layer of elastic membrane is coated on the origami shoulder for multiple functions. First, the elastic membrane can seal the origami mechanisms to ensure that there are no air gaps/pores thus achieving efficient actuation by pneumatic pumps. Second, elastic membrane helps to store elastic energy that can be applied to rapidly deploying the compliant origami, allowing a fast response to improve the motion speed. Third, the elastic membrane is hydrophobic which ensures the structural stability of origami shoulder in water because the raw paper material is hydrophilic and will swell to lose its structure.

In addition, the strain sensing capability is integrated onto the octagon-origami structures by coating a conductive polymer of poly (3,4-ethylenedioxythiophene)-poly (Styrenesulfonate) (PETDOT:PSS), as shown in Fig.1. The polymer coating tightly adheres to the octagon-origami structures through the strong covalent bonds between PETDOT:PSS and cellulose fibers. As a result, the origami robot demonstrates the sensing capability during the actuation period through perceiving the electronic signal changes under small body deformations, which can be used for obstacle detection.

After the origamis are selected, detailed analysis is

implemented to seek the most efficient actuation and control system. Here, a pneumatic control strategy of time division, multiplexing, and serialization is applied to driving the origami joints. Basically, robot joints are driven by customized pneumatic units (under the control of the microcontroller) which can exhaust or inhale based on different time segmentations named ‘time-division’. According to the decomposition of robot crawling, turning, and swimming, we achieve an optimal solution that uses only four pneumatic units to drive eight robot joints, which is called ‘multiplexing’. The front and rear legs are driven by one pneumatic unit. The synchronous motion of the front and rear legs enables the robot to crawl while the differential actuation among the legs makes the robot turn. Another two pneumatic units drive the six joints of the robot arms to swim. In terms of robot control, a simple but effective control logic strategy named ‘serialization’ is proposed based on the finite state machine (every pneumatic unit has three states: exhaust, inhalation, and non-working). Each robot motion is realized by a specific combination of the different states of the pneumatic units.

### B. Construction of the proposed robot

#### 1) Design of octagon-origami structures and robot legs

An octagon-origami structure combined with robot legs is designed as a simple mechanism to transform body deformation to linear motion for a crawling gait, which is similar to an earthworm with anisotropic friction and has been adopted in other origami-inspired robots with similar gaits[20].

The main objective of this section is to construct origami-based structures that are capable of driving the robot legs to cause the robot’s crawling and turning gaits. We consider that the origami module here must present the same bending capabilities, allowing the robot to realize the proposed gaits on the ground. Furthermore, not only the fast foldability but also a simple fabrication is required to apply an origami-based structure. The octagon-origami structure is adopted as the actuation mechanism for keeping the same functionality and control schemes[21]. The octagon-origami structure is considered a beam that can be bent, which is actuated by a pneumatic system. The interaction forces between the legs on the robotic body and the ground, including the reaction forces and friction forces, enable the front and rear legs to roll on a contact surface. The bending deformation of octagon-origami structures (robotic body) raises once the air pressure is imposed on these two octagon-origami structures for generating bending moments, which results in the changes of interaction forces. Thus, the rolling and dragging motion phases for a general crawling gait are transmitted according to the bending moments.

The origami structure described here achieves the proposed performance with a scalable, rapid, and cost-effective manufacturing process. The origami structure of the robot body is made up of a series of octagon-origami blocks, as shown in Fig.2. The 3D printed front and rear legs are connected to two octagon-origami structures. Due to the contact friction with the ground, two octagon-origami structures are driven by the pneumatic pump with the same bend frequencies to generate the pitch angle. Each foot of the front and rear legs have two surfaces with different frictional coefficients. The front feet possess a smooth and rounded surface with a low coefficient of friction, while the back feet

surface is with a high coefficient of friction. For such a design, there are three advantages as follows. When the robot moves, the feet tilt forward between these faces so that the smooth surface facilitates forward sliding and the rough surface prevents backslide, as shown in Fig.2.

In particular, the air inflation causes expansions of octagon-origami structures, enabling the front feet to slide forward while the friction surfaces on the rear feet prevent backslide of the robot forcing it to expand in the forward direction. Due to the air inspiration, the robot body is shrunk in length, allowing the rear feet to rock onto the smooth surface and then, slide towards the front feet. In the next stage, the friction surface on the front feet rocks backward to engage with the ground to prevent backslide of the front face of the robot. Through periodic and alternated action stages, the robot can crawl and turn. Changing the lengths of two octagon-origami structures by different signal frequencies determines the direction of crawling. Left and right turnings are facilitated using two independently driven octagon-origami structures mounted at the front and rear legs. By contracting the left octagon-origami structure and repeatedly expanding and contracting the right one, the robot is made to turn left as shown in Fig.2, and vice versa to turn right.

## 2) Shoulder design

### *Design of origami twisted tower*

The traditional Kresling pattern is designed as a flat-foldable mechanism, that is, its length at a fully folded stable state is exactly zero[22]. We propose and describe a “generalized” Kresling pattern called the origami twisted tower that can be tailored to feature a non-zero length at a fully-folded state. Here we design an origami twisted tower: the base and top are square, which twists 90°. When opening up, it twists itself, causing the change of the height, as shown in Fig.3(A). The corresponding crease pattern consists of the equally spaced mountain and valley creases. The first and last valley creases are glued together to generate a rotationally symmetric twisted polygonal prism. The base and top of the regular polygons are considered rigid during the folding motion. The resulting crease pattern is no longer flat foldable but retains an identical range of rotation as viewed from the top. An origami mechanism is rigidly foldable if all facets remain flat and rigid throughout the folding motion. The origami structure can be uniquely defined by the three parameters, the number  $n$  of sides of the basal polygon, the circumradius  $R$  of the basal polygon, and the helical angle ratio  $\lambda$ , respectively. Based on these parameters, the basic polygon relations are easily determined. In addition, a higher angle ratio corresponds to stronger stability. The design mathematical model of the origami tower is provided in the supplemental material.

### *Combination of origami twisted towers*

By combining the origami twisted towers in the 3D space, we can obtain the origami structure with a large range of rotation angles or multiple DOFs. To realize any twisted angle, we use a chain of serially connected, generalized origami twisted towers as a driving module to demonstrate the use of rotation. For the origami twisted tower with  $n$ -side polygon base, the maximum angle is  $360^\circ/n$ . We also examine the maximum rotation angles by constructing the origami twisted towers and combining them in serial. For instance, the serial origami towers can rotate  $\pm 360^\circ$ , as demonstrated in Fig.3(A).

Moreover, the origami structure can realize the pitch, yaw, and roll motions by configuring the spatial positions of the origami twisted towers (see Fig.3-A). By combining the origami twisted towers, we can theoretically drive the robot to realize any complex motion with multiple DOFs.

In this work, one of the major challenges is developing a robot that is capable of swimming on the water surface for supporting the robot’s weight by paddling the water. Previously developed water strider-inspired robots[23, 24] rely on multiple, non-moving legs to support themselves on the water surface. Such designs limit the robots’ ability to move in terrestrial scenarios. Here, we design a structure based on the combination of origami twisted towers without non-moving legs, allowing for multimodal locomotion on the group and water surface.

The proposed robot uses the designed shoulders and arms to move on the water surface symmetrically, imitating the swimming humans and the diving flies (*Ephydria hians*), as illustrated in Fig.3. Previous biomimetic studies analyzed the human’s breaststroke paddling arm-hand trajectories and showed that the human’s arm-hand contacting the shoulder completes the rotation motion while forth-and-back moving[25]. In particular, the humans perform breaststroke on the water surface by paddling their arm-hands symmetrically to generate unidirectional thrust. During the power stroke, the hand palm flattens to increase the contact area with water to improve forward thrust. During the recovery stroke, the arm and hand palm retract to minimize the contacted area and reduce backward drag. In addition, in terms of the force equilibrium, the arm-hand of a human presses the water with a certain inclination to provide the thrust and lift.

Taking inspiration from human physiology and swimming mechanics, we develop an active swimming origami mechanism that generates symmetric gaits for water surface locomotion, as shown in Fig.3(D, E, F, G).

The robot shoulder consists of three origami twisted towers, which allows the robot arm to realize 3D motions (see Fig.3-B). The shoulder motion is controlled, and the flap rotation is passively mediated through the arm. In the water, the robot shoulder firstly rotates its arm around 90° by the base joint and then, moves around 90° through the outreaching joint (see Fig.3-D, E, F, G). Indeed, the origami twisted tower can generate linear and rotation motions simultaneously, which is similar to the waving human’s arm-hand extending-retracting and rotating. Moreover, for the rotation joint, we allow the arm to rotate about 90° so that the motion is inclined to the water surface for providing the forward thrust and the lift, as illustrated in Fig.3(F, G). During the backward paddling, the origami surfaces of the arm remain fully open to generate forward thrust; its direction is almost vertical to the water surface. During the forward paddling, the origami surfaces of the arms collapse to reduce drag and rotate to the direction parallel with the water surface. Consequently, developing an appropriate swimming motion for the robot is crucial for achieving desired swimming kinematics.

## 3) Body sensor

In this work, we integrate poly(3,4-ethylenedioxythio phene)-poly(styrenesulfonate) (a conductive polymer, abbreviated as PETDOT:PSS) with cellulose paper as conductive coating to realize the built-in strain sensing capability of the fabricated origami robot. In particular,

cellulose paper is soaked into PETDOT:PSS (1.3 wt % dispersion in water). After air drying, as shown in Fig. 4(A), the surface color changes from white to dark blue, while the porous cellulose fibers are covered by a thin layer of PETDOT:PSS coating. According to the scanning electron microscope (SEM) images in Fig. 4(B, C), the thickness of PETDOT:PSS coating is about 3  $\mu\text{m}$ . By repeating the soaking and drying process, one can easily coat conductive PETDOT:PSS layer onto various origamis. Herein, two octagon-origami structures are coated by PETDOT:PSS and assembled as the robotic body (see Fig.4-D). Due to the ultra-thin coating, the octagon-origami structure is not affected and robotic weight change is also ignorable (< 0.1%), which are a great benefit for next-generation power efficient and sustainable soft robot.

Our PETDOT:PSS coated origami robot shows built-in strain sensing capability. The robot is actuated by the proposed pneumatic system, which experiences repeated deflated and inflated states to crawl forward. Under the deflated state, in Fig. 4(E), the octagon-origami is compressed, and surface cracks emerge on the ridges of origami folds thus leading to higher resistance. When transiting to an inflated state, origami folds are flattened. As a result, surface cracks are recovered and conductive pathways are re-connected (Fig. 4-E), which causes reduced resistance. During the repeated robotic actuation, as shown in Fig.4(F), real-time sensing signals are obtained to reflect the robotic body deformations. Both the baseline and peaks of sensing signals keep stable due to the strong covalent bonds between PETDOT:PSS and cellulose fibers.

#### 4) Robot control

We use customized pneumatic units to drive the robot joints. Each unit is composed of two sets of motors and air pumps, one of which is for exhaust and the other for inhalation. The air pump can provide sufficient air pressure to flex and extend the joint. The airflow can be adjusted to adapt to different motion speeds. The microcontroller controls the exhaust and inhalation of the units by deciding which air pump to work. The time interval  $t$  between the switching of pumps determines the motion speeds. The map between the units and the robot joints is as follows. The outreaching joints (left and right) and the rotation joints (left and right) share one unit (see Fig.5-A) since their movements are synchronous during swimming. The units B and C drive the left and right legs of the robot, respectively. Unit D drives the left and right base joints since their movement is synchronous as well.

In terms of the operation, the crawling straight motion is completed by the synchronous inhalation and exhaust of units B and C. When one of the units B and C is always inhaling, and the other is alternately inhaling and exhausting, the left and right legs of the robot move differentially to turn. For swimming, unit D first inhales to lift the robot arms. Then, unit A alternately inhales and exhausts to stroke the robot arms to swim. At the end of swimming, unit A stops working and unit D exhausts to put down the robot arms.

### C. Experiments

To validate that the proposed robot can perform the locomotion gaits in environments, we conduct the corresponding locomotion experiments: independent gait tasks across the three gaits: crawling, turning, and swimming,

for various power conditions. We study the robot's motion via recording each experiment employing a camera with video recording for locomotion gaits and tracking the chosen point via the video analysis software (Tracker).

#### 1) Crawling gait

The control of the joints consisting of the octagon-origami blocks allows repeatable regulation of the crawling step size; hence, the total travel distance of the robot can be defined before crawling. The pneumatic actuators drive the octagon-origami to generate the deformation for causing the crawling gaits of the front and rear legs.

To test the effectiveness of the crawling gait, we guide the proposed robot via the pre-programming to perform the straight-line and turning maneuverability on the flat surface, as demonstrated in Fig.6 and Fig.7. The front legs are moving forward, and the rear legs are blocked by the friction and then, the front legs are blocked, and the rear legs move forward in the next stage. The crawling time and distance are measured by the Tracker program.

The proposed robot completes an average repeatable step of an average of 0.25cm/s on the flat surface with the 0.33Hz crawling gait, but the steps sometimes are not repeatable. This is probably due to multiple potential factors such as actuation nonlinearity, sliding caused by imperfect sticking of the legs, compliant combinations of origami structures, and poor leg-ground contact with the surface, which causes slippage. In Fig.6(B, F), the three snapshots that illustrate the robot crawls are combined, representing the footages of the robot at an equal constant interval. The trajectories of Fig.10-1(A) are smooth and repeatable.

Figure 7 demonstrates the proposed robot scalability for effectively turning. When turning maneuverability, the robot needs to do morphologic deformation, allowing two actuated octagon-origami structures to have different lengths for realizing the differential motions. As for the cases of Fig.7, their displacements and velocities are shown in Fig.10-2 for the left-turning and right-turning, respectively. The linear velocity has drastic impulses during the crawling period since the crawling motion is generated from the friction peristalsis (see Fig.10-2-B). The motion circles remain almost repeatable for the proposed robot system.

#### 2) Obstacle detection via the body sensor

We implement the experiments to validate that the built-in body sensor can detect the collision between the robot and an obstacle, which potentially can be integrated into the closed-loop robotic control. The robot body experiences repeated deflated and inflated states when crawling forward, where the body sensor continuously provides resistive signals. Upon colliding an obstacle, the deformation scale of the robot body is different from that of the robot crawling forwards since the front leg is unable to move, resulting in a bend up of the robotic body. As shown in Fig.8(A), the angles of the origami body at the inflated state are 83° and 80° before and after the collision, respectively. The upward bending of the octagon-origami structures at 80° may induce better recovery of surface cracks which leads to smaller resistance. As shown in Fig.8(B), when the robot crawls forward before collision (we recognize it as stage 1), the relative resistance change of the body sensor is from 0 to -9.47%. After the robot meets an obstacle (recognized as stage 2), the signals of the body sensor show a lower baseline at -9.71%. With such electrical

feedback by the minor body deformation, we demonstrate that the robot is capable of detecting the front obstacle and makes a decision to stop the actuation. The avoidance process is clearly illustrated in Fig.8.

### 3) Swimming

We demonstrate that the proposed robot is capable of swimming locomotion by imitating human's swimming behaviors. Figure 9 captured by the camera on the top view illustrates a swimming scenario where the proposed robot attempts to arrive at the end of the water tank. Initially, the robot locates on the left side. The shoulders and arms of the robot are controlled by the same signal such that they generate the almost symmetric kinematic morphologies.

The robot swims with an average speed of 0.66cm/s (0.11 main body length (BL) per second) on the water surface, provided by the 0.33Hz swimming gait. As the weight of the robot is small (60 g), the robot can move on the water surface, which also results in lightly drifting within 2cm along the  $x$  direction, moving forward 20cm along the  $y$  direction. The maximum swimming speed is 4.2cm/s (0.7 BL per second) along the moving direction, as shown in Fig.10-3(A). Figure 10-3(B) indicates that the robot generates an instantaneous velocity in the opposite direction. This is somewhat expected since the robot hands push water forward while the outreaching joints retrieve.

Specifically, when the shoulders with arms push water backward, the origami surfaces bend to cover more water, thus increasing thrust. In addition, the elastic membrane (a thin layer of Ecoflex elastomer) used in the origami surface stretches and stores energy that can be rapidly released to assist the arms to return the initial state.

## 3. Conclusion

Our presentation of a bio-inspired mesoscale-legged robot capable of locomotion included an origami-based design that allowed us to control the folding and unfolding of the robot for achieving controllable, repeatable multi-locomotion on terrestrial and aquatic domains. Our design almost satisfied the various constraints from the weight, low cost, the deployment in different environments, and so on. For instance, although the lightweight and low-cost constraints led to conflicting design requirements, they could be suitably reconciled by leveraging the advantage of the origami structural variety. The design of the differential octagon-origami structures enabled the front-rear legs of the robot to crawl straight, turn the left and right. Moreover, using a space combination of origami twisted towers, we developed the origami shoulders to realize aquatic flapping locomotion. The study of the combination of different kinds of origami towers will also provide insight into constructing modular robots such as industrial robotic arms (Supplementary material). In particular, for each DOF, the origami twisted towers configured in the serial can rotate at the range between  $\pm 360^\circ$ . For each joint, two serial tower groups are combined in the 3D space, which enables the joint to perform two-directional motions, including linear stretch and rotation. Further, we designed a pneumatic control system of time division, multiplexing, and serialization, which was able to drive the origami structures to fold and unfold. The resulting assembly was validated and performed a variety of locomotion tasks.

In addition, as a demonstration of a potential application for environment inspection, we performed the experiment of the robot detecting obstacles through the body sensor. Instead of adding electronic sensors onto the robot, we built a conductive PETDOT:PSS integrated origami backbone. Without any extra electronic module, the conductive origami backbone itself was capable of sensing the strain changes from body deformations. We successfully demonstrated that the built-in sensing capability could be applied to detecting front obstacles during robotic locomotion.

Considering the bio-inspired origami design, integrated body sensing, multi-modular origami coordination, followed by the motion control of multiplexing, time-division, and serialization to finally reach the amphibious soft machine, we expect this work demonstrates contributions to advanced origami robot design, body sensor, and actuation control for broadly practical applications.

Referring to the insight of combining different origami structures, we can allow a robot to achieve more complex locomotion gaits than the ones mentioned in this work. For instance, by swapping the left and right arms, the proposed robot can be considered as a mobile manipulation platform, which is used in grasping light plastic bags and packing boxes. The octagon-origami structures drive the robot to head a destination while two arms with origami twisted towers hold an object. In terms of the proposed body sensor, it also can be used in origami twisted towers; however, there is a high risk that water backflows into the robotic body during the pneumatic actuation in water. In experiments, we used silicone elastomer to seal the origamis, yet the adhesion energy between silicon and PEDOT:PSS in the water is not very strong. As a result, during actuation in water, the silicon layer is possibly detached, which causes the water backflow. Therefore, we did not include sensor design in the origami twisted tower. An alternative approach to addressing this issue is to avoid silicon/(PEDOT:PSS) interface, which could achieve by coating PEDOT:PSS only onto the inner surfaces of paper origamis and we seal the outer surface with silicon. Moreover, although it is found that the signal difference is small before and after the obstacle in experiments, the proposed robot still could get the corresponding feedback of a detected obstacle. However, to improve the capability of the robot detecting obstacles, we propose potential solutions, including the designs of the sensor circuit, sensing material as well as origami structure, for enlarging the signal difference. First, we can use an amplifying circuit to enlarge this signal difference. Second, we can adopt thicker paper to fold the origamis. After coating PEDOT:PSS, the relative resistance changes will be larger with response to deformations, as the thicker paper substrate would induce larger surface cracks during bending. Third, the octagon-origami structure can be re-designed to make it easier to deform when the robot meets an obstacle. With larger body deformations, the sensor signal difference will be enlarged.

Future studies will focus on a few topics to further improve robot locomotive capabilities in complex scenarios. The proposed prototype without the capability of underwater locomotion may flip over in presence of disturbances such as surface waves and dynamic flow underwater. Thus, we plan

to study the robot's dynamics during underwater locomotion to explore alternative gaits for robotic swimming. Future research could involve enabling the capability of swimming under the water. To address this limitation, we may optimize the robot's gait to realize morphological changes through a suitable buoyancy control strategy, compliance in the backbone [26], and/or an active tail[27]. Future work also could endow propellers that extend the robot to be capable of flying in the air. Ultimately, we hope that these improvements can one day allow robots to seamlessly navigate complex 3D surfaces much like their biological counterparts.

## Contribution Statement

The first four authors take charge of building the robot, performing the experiments and writing the manuscript; Haoyong Yu provides a high research insight.

## Author Disclosure Statement

No competing financial interests exist.

## Funding Information

This work was supported by Agency for Science, Technology and Research, Singapore, under the National Robotics Program, with A\*star SERC Grant No.: 192-25-00054.

## References

- [1] J.-S. Koh et al., "Jumping on water: Surface tension-dominated jumping of water striders and robotic insects," *Science*, vol. 349, no. 6247, pp. 517-521, 2015.
- [2] M. Wehner et al., "An integrated design and fabrication strategy for entirely soft, autonomous robots," *Nature*, vol. 536, no. 7617, pp. 451-455, 2016.
- [3] M. A. Robertson and J. Paik, "New soft robots really suck: Vacuum-powered systems empower diverse capabilities," *Science Robotics*, vol. 2, no. 9, 2017.
- [4] J. Fan, S. Wang, Q. Yu, and Y. Zhu, "Swimming performance of the frog-inspired soft robot," *Soft robotics*, vol. 7, no. 5, pp. 615-626, 2020.
- [5] Y. Chen, N. Doshi, B. Goldberg, H. Wang, and R. J. Wood, "Controllable water surface to underwater transition through electrowetting in a hybrid terrestrial-aquatic microrobot," *Nature communications*, vol. 9, no. 1, pp. 1-11, 2018.
- [6] S. Won, S. Kim, J. E. Park, J. Jeon, and J. J. Wie, "On-demand orbital maneuver of multiple soft robots via hierarchical magnetomotility," *Nature communications*, vol. 10, no. 1, pp. 1-8, 2019.
- [7] C. S. X. Ng, M. W. M. Tan, C. Xu, Z. Yang, P. S. Lee, and G. Z. Lum, "Locomotion of Miniature Soft Robots," *Advanced Materials*, p. 2003558, 2020.
- [8] Y. Tang, Q. Zhang, G. Lin, and J. Yin, "Switchable adhesion actuator for amphibious climbing soft robot," *Soft robotics*, vol. 5, no. 5, pp. 592-600, 2018.
- [9] A. D. Marchese, C. D. Onal, and D. Rus, "Autonomous soft robotic fish capable of escape maneuvers using fluidic elastomer actuators," *Soft robotics*, vol. 1, no. 1, pp. 75-87, 2014.
- [10] Y. Tang et al., "Leveraging elastic instabilities for amplified performance: Spine-inspired high-speed and high-force soft robots," *Science Advances*, vol. 6, no. 19, p. eaaz6912, 2020.
- [11] H. Yuk, D. Kim, H. Lee, S. Jo, and J. H. Shin, "Shape memory alloy-based small crawling robots inspired by *C. elegans*," *Bioinspiration & Biomimetics*, vol. 6, no. 4, p. 046002, 2011.
- [12] S. Felton, M. Tolley, E. Demaine, D. Rus, and R. Wood, "A method for building self-folding machines," *Science*, vol. 345, no. 6197, pp. 644-646, 2014.
- [13] W. W. Lee et al., "A neuro-inspired artificial peripheral nervous system for scalable electronic skins," *Science Robotics*, vol. 4, no. 32, 2019.
- [14] T. Kim, S. Lee, T. Hong, G. Shin, T. Kim, and Y.-L. Park, "Heterogeneous sensing in a multifunctional soft sensor for human-robot interfaces," *Science Robotics*, vol. 5, no. 49, 2020.
- [15] D. Rus and M. T. Tolley, "Design, fabrication and control of origami robots," *Nature Reviews Materials*, vol. 3, no. 6, pp. 101-112, 2018.
- [16] B. Shih et al., "Electronic skins and machine learning for intelligent soft robots," 2020.
- [17] H. Yang et al., "Wireless Ti3C2T x MXene Strain Sensor with Ultrahigh Sensitivity and Designated Working Windows for Soft Exoskeletons," *ACS nano*, vol. 14, no. 9, pp. 11860-11875, 2020.
- [18] S. Miyashita, S. Guitron, M. Ludersdorfer, C. R. Sung, and D. Rus, "An untethered miniature origami robot that self-folds, walks, swims, and degrades," in *2015 IEEE International Conference on Robotics and Automation (ICRA)*, 2015: IEEE, pp. 1490-1496.
- [19] Z. Zhakypov, K. Mori, K. Hosoda, and J. Paik, "Designing minimal and scalable insect-inspired multi-locomotion millirobots," *Nature*, vol. 571, no. 7765, pp. 381-386, 2019.
- [20] J.-S. Koh and K.-J. Cho, "Omega-shaped inchworm-inspired crawling robot with large-index-and-pitch (LIP) SMA spring actuators," *IEEE/ASME Transactions On Mechatronics*, vol. 18, no. 2, pp. 419-429, 2012.
- [21] L. Paez, M. Granados, and K. Melo, "Conceptual design of a modular snake origami robot," in *2013 IEEE International Symposium on Safety, Security, and Rescue Robotics (SSRR)*, 2013: IEEE, pp. 1-2.
- [22] A. Pagano, T. Yan, B. Chien, A. Wissa, and S. Tawfick, "A crawling robot driven by multi-stable origami," *Smart Materials and Structures*, vol. 26, no. 9, p. 094007, 2017.
- [23] K. Suzuki, H. Takanobu, K. Noya, H. Koike, and H. Miura, "Water strider robots with microfabricated hydrophobic legs," in *2007 IEEE/RSJ International Conference on Intelligent Robots and Systems*, 2007: IEEE, pp. 590-595.
- [24] Y. S. Song and M. Sitti, "STRIDE: A highly maneuverable and non-tethered water strider robot," in *Proceedings 2007 IEEE International Conference on Robotics and Automation*, 2007: IEEE, pp. 980-984.
- [25] D. Chollet, L. Seifert, H. Leblanc, L. Boulesteix, and M. Carter, "Evaluation of arm-leg coordination in flat breaststroke," *International journal of sports medicine*, vol. 25, no. 07, pp. 486-495, 2004.
- [26] K. L. Hoffman and R. J. Wood, "Robustness of centipede-inspired millirobot locomotion to leg failures," in *2013 IEEE/RSJ International Conference on Intelligent Robots and Systems*, 2013: IEEE, pp. 1472-1479.
- [27] S. Kim, M. Spenko, S. Trujillo, B. Heyneman, D. Santos, and M. R. Cutkosky, "Smooth vertical surface climbing with directional adhesion," *IEEE Transactions on robotics*, vol. 24, no. 1, pp. 65-74, 2008.

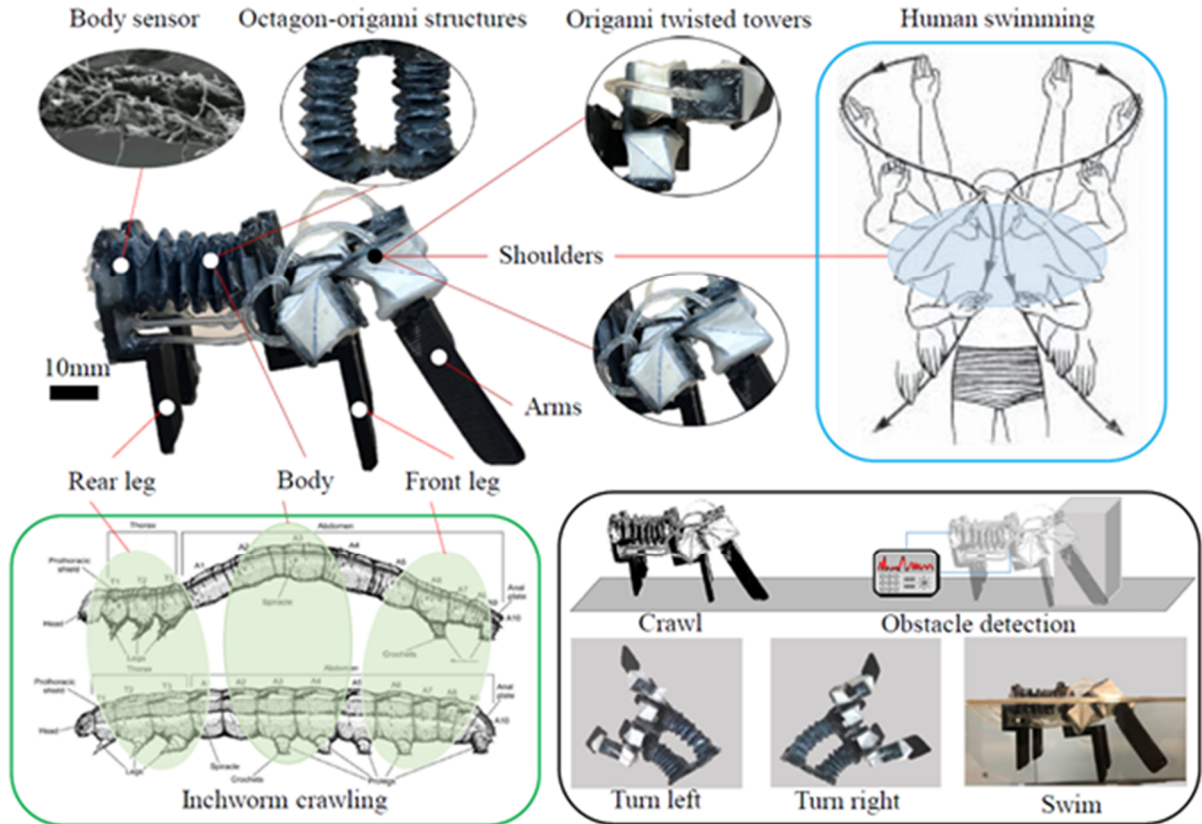


**Figure 1.** The design and multi-locomotion gaits of the bio-inspired origami robot with body sensing. The picture titled ‘body sensor’ shows the texture of body sensor; the robotic body is made up of two octagon-origami structures; origami twisted towers consist of robotic shoulders; the origami robot imitates the inchworm crawling gait shown in the green frame and the human swimming behaviors illustrated in the blue frame; the proposed robot crawling, turning, swimming and obstacle detection based on the coated body sensor demonstrated in the black frame.

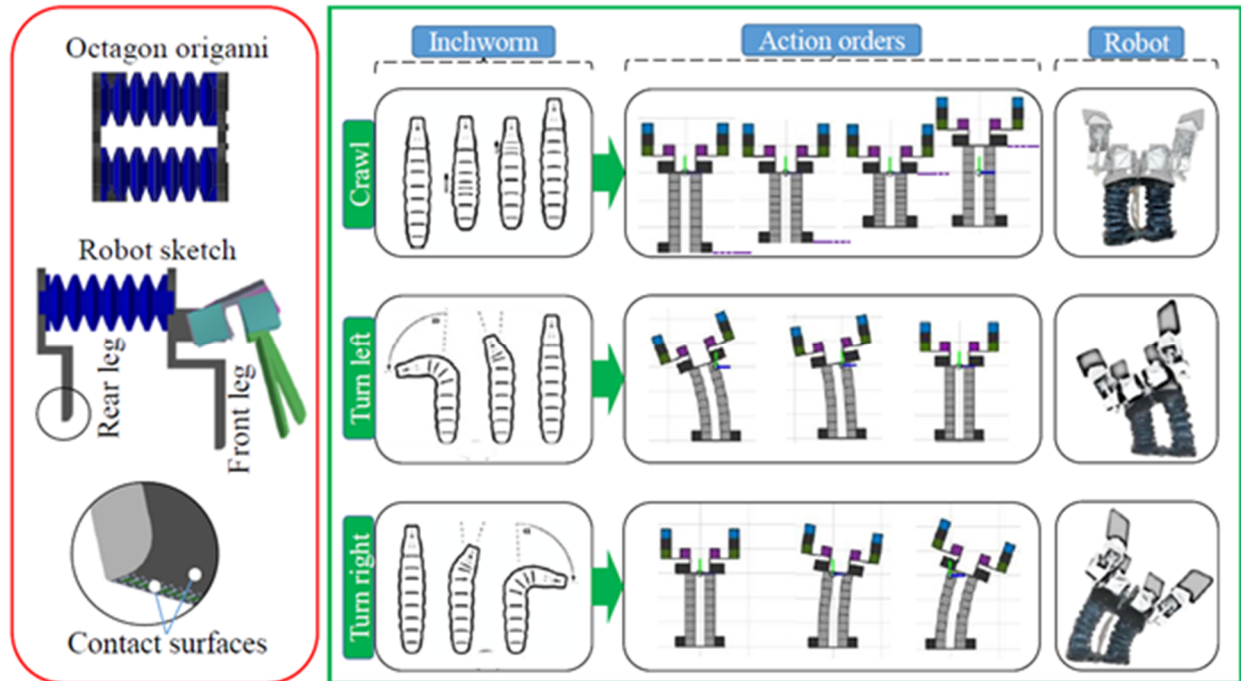


**Figure 2.** The robot sketch in the red frame; the robot crawling in the first row, turning left and right in the second and third rows respectively in the green frame. Note that the turning gait also belongs to the crawling gait. The inchworm locomotion gaits of crawling and turning in the first column; the second column shows the crawling and turning gait simulations; the third column illustrates the real robot crawls and turns.

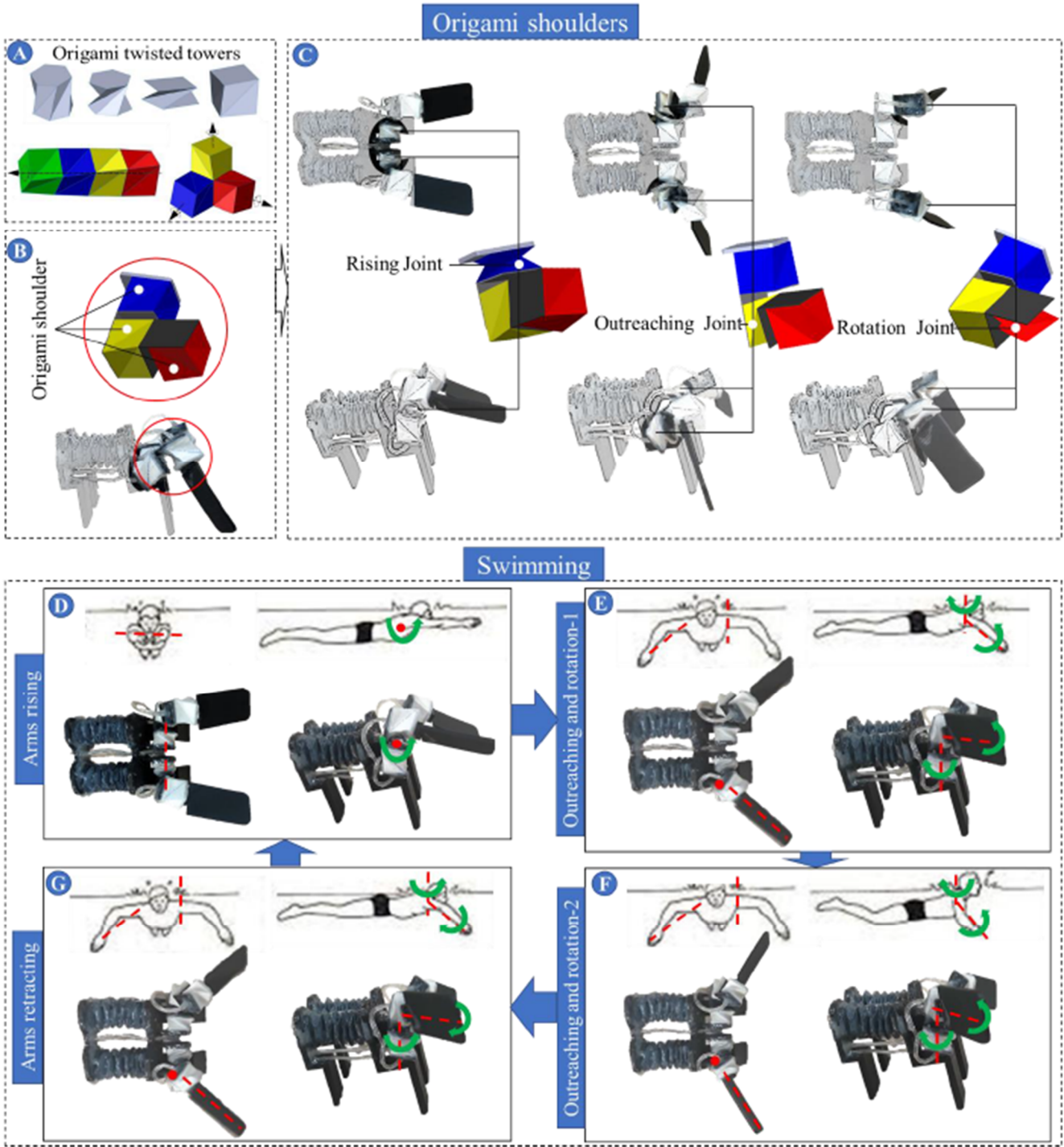


**Figure 3.** Origami twisted towers (A), the shoulder design based on the combination of the designed origami twisted towers(B) and the change of joint configuration of the shoulder(C). The diagram in a red circle is the shoulder with 3 DoFs; the blue, yellow and red origami twisted towers are the rising, outreaching and rotation joints, respectively(B). The diagram named ‘Swimming’ illustrates the swimming circle with the action decomposition of human swimming. The power stroke and the recovery stroke are asymmetric. The base joints raise the robot arms. From (D) to (E), the outreaching and rotation joints synchronously rotate. From (E) to (F), these two joints continuously rotate. From (F) to (G), the shoulders and arms turn to the next motion circle.

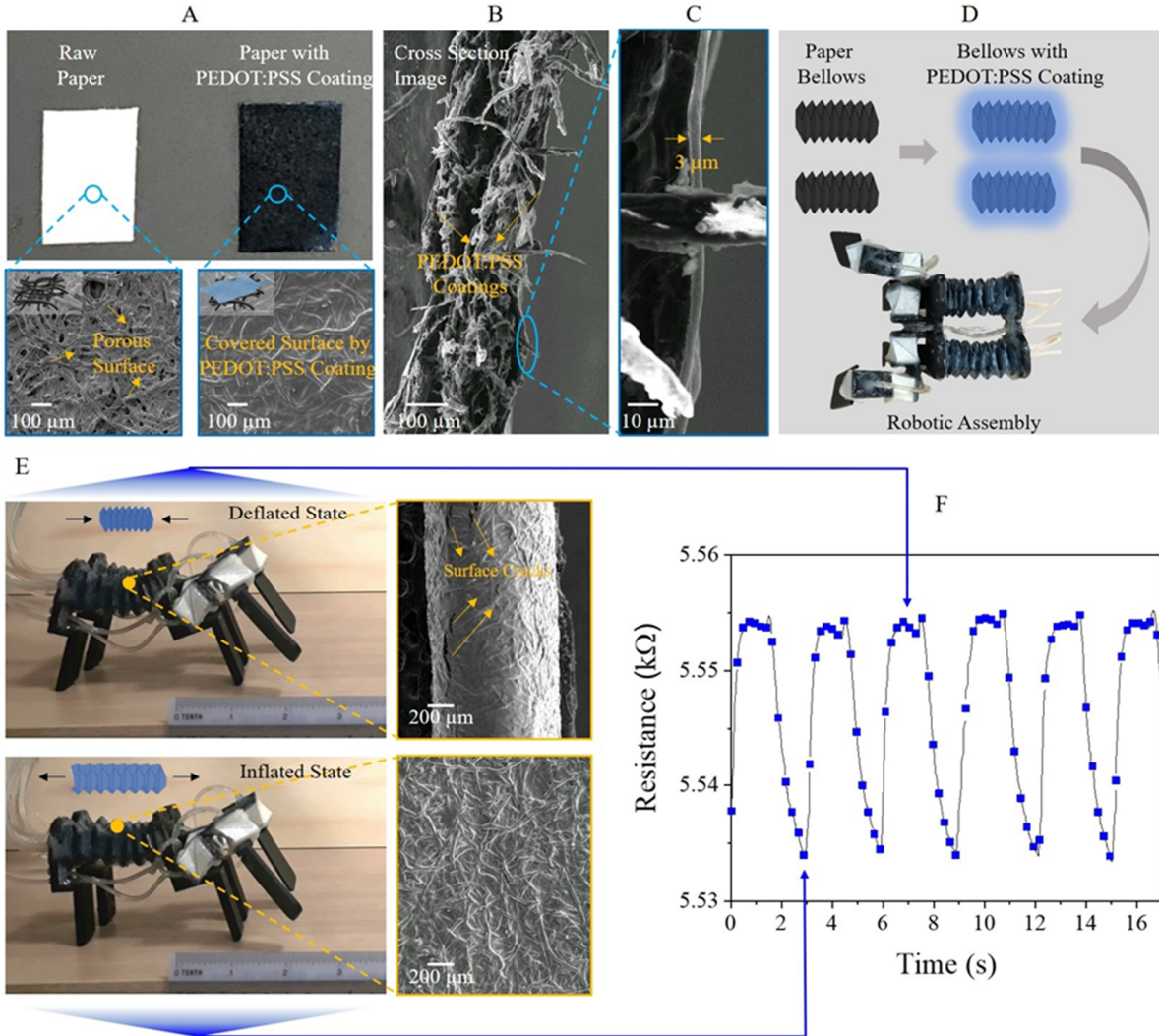


**Figure 4.** Built-in strain sensing capability of origami robot. (A) Digital and SEM images of cellulose paper before and after PEDOT:PSS coating. (B) Cross section SEM image of PEDOT:PSS coated paper. (C) Amplified high-resolution SEM image at cross section of PEDOT:PSS coated paper. (D) Fabrication of conductive octagon-origami structure and robotic assembly. (E) Robotic actuation at deflated and inflated states and corresponding SEM images of PEDOT:PSS coating at the ridge of origami fold. (F) Real-time resistance signal of robotic body while moving forward.

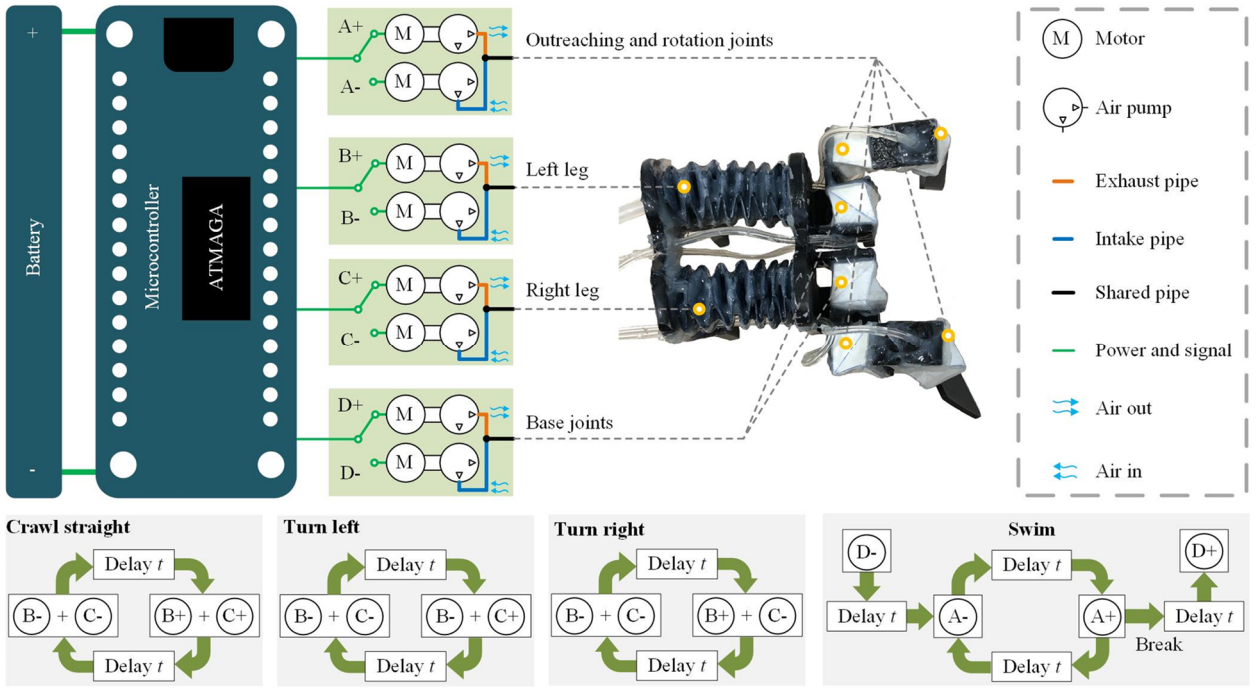


**Figure 5.** The actuation and control system of the proposed robot. Robot joints are driven by four customized pneumatic units (A, B, C and D) composed of motors and air pumps. Each unit can exhaust or inhale under the control of the microcontroller. When one unit exhausts (represented by A+, B+, C+, D+) or inhales (represented by A-, B-, C-, D-), the corresponding robot joint(s) extends or flexes. The crawling, turning and swimming motions are completed by different combinations of the units' inhalation and exhaust. The time delay  $t$  determines the speed of the motions.

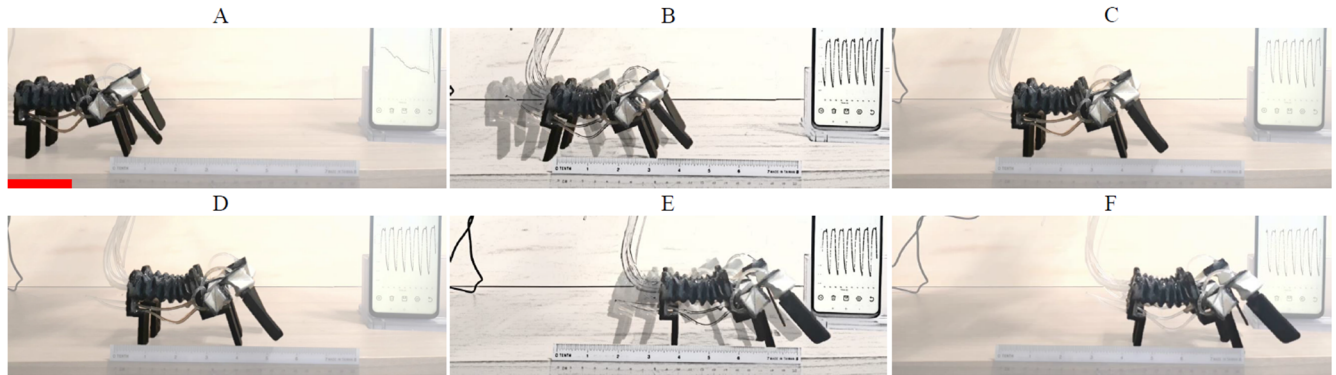


**Figure 6.** The proposed robot crawls on the ground from A to F, including the starting statuses (A, D) and the ending statuses (C, F), the snapshots while crawling with the equal time interval(B, E). Scale red bar, 5 cm.

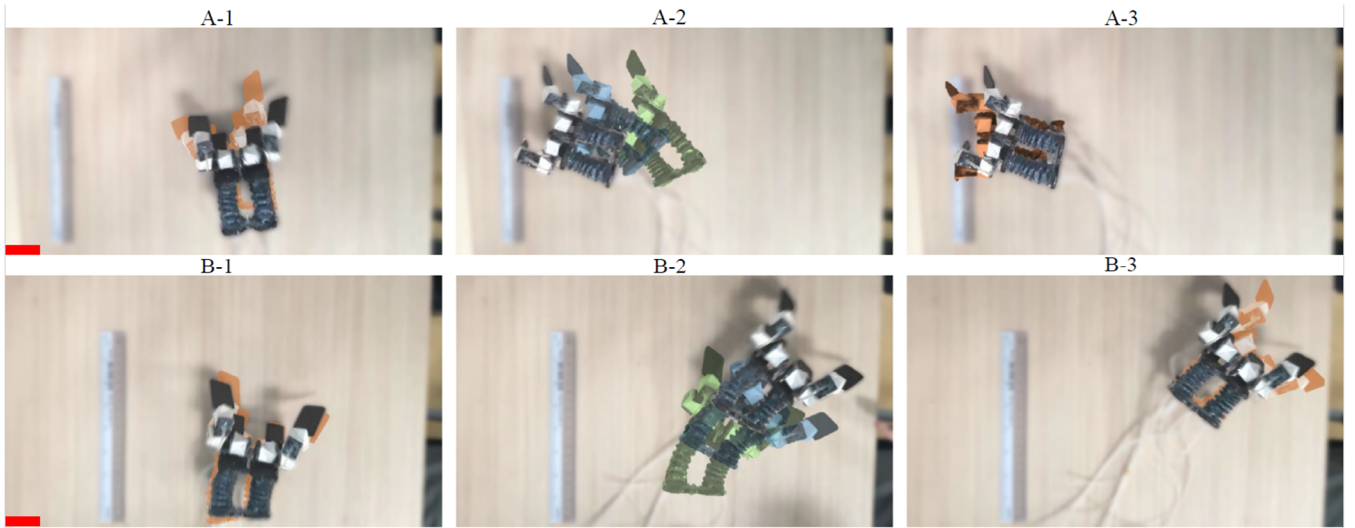


**Figure 7.** The robot turning left(A) and turning right(B), respectively. Scale red bars, 5cm.

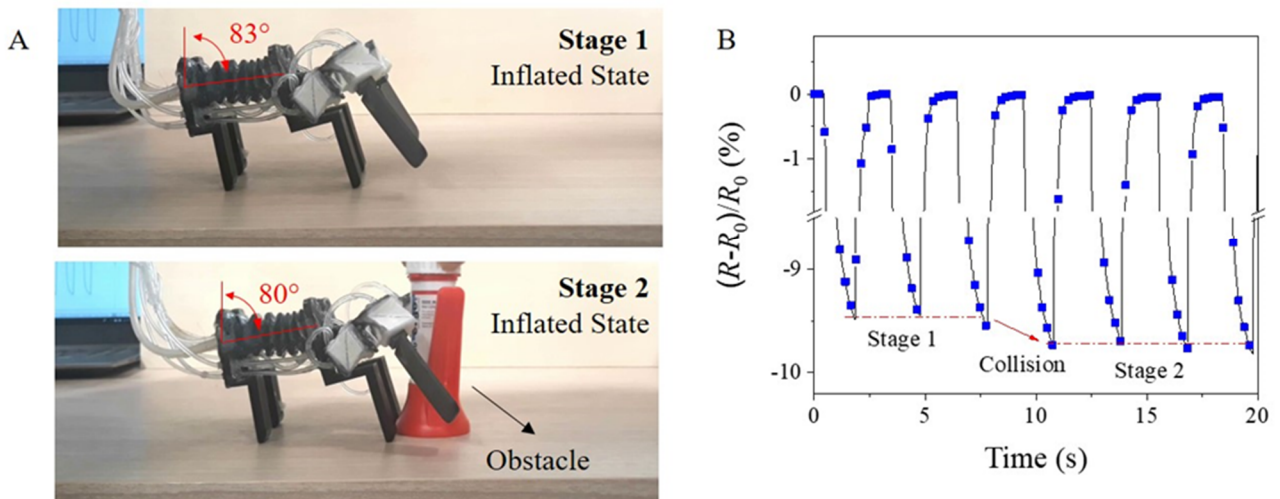


**Figure 8.** Obstacle detection via the body sensor. (A) Robotic actuation at inflated state before and after meeting the obstacle. (B) Relative resistance changes from body sensor before and after meeting the obstacle.  $R_0$  and  $R$  are original resistance and resistance under actuation, respectively.

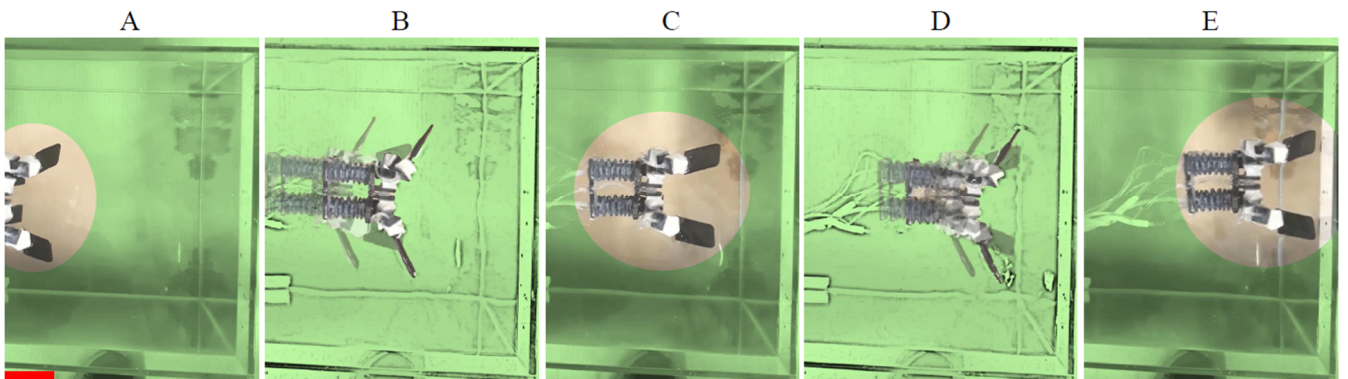


**Figure 9.** Robot swimming in a water tank from the top view. The starting(A), middle(C) and ending(E) statuses. (B) and (D) represent the continuous swimming actions. Scale red bar, 5cm.

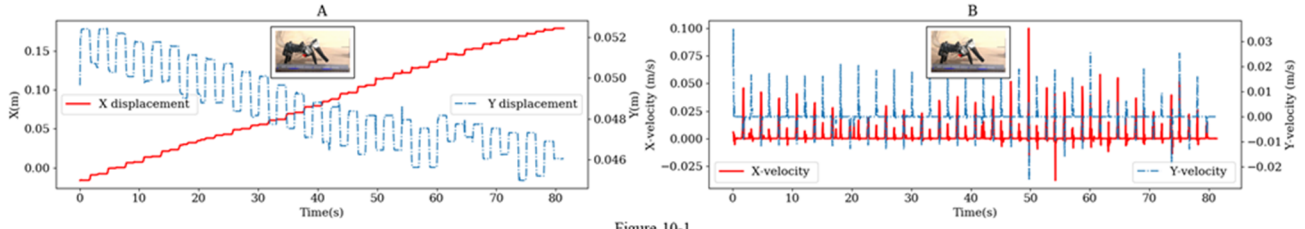


Figure 10-1

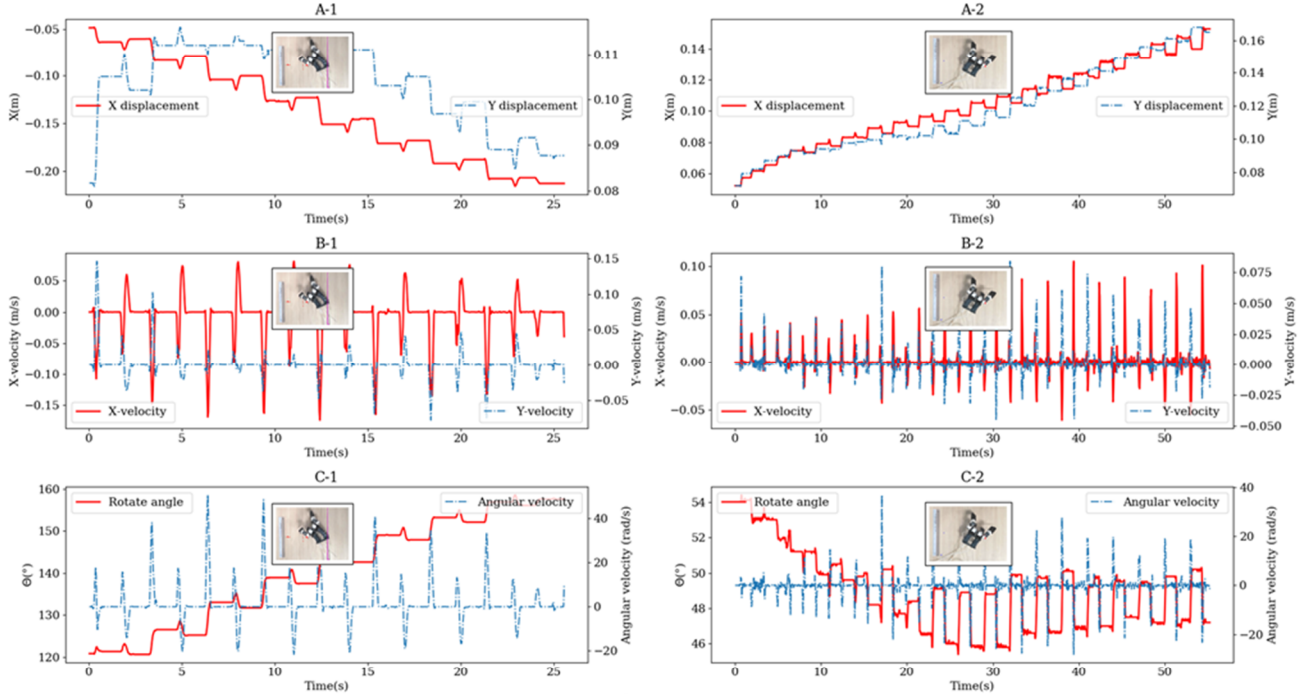


Figure 10-2

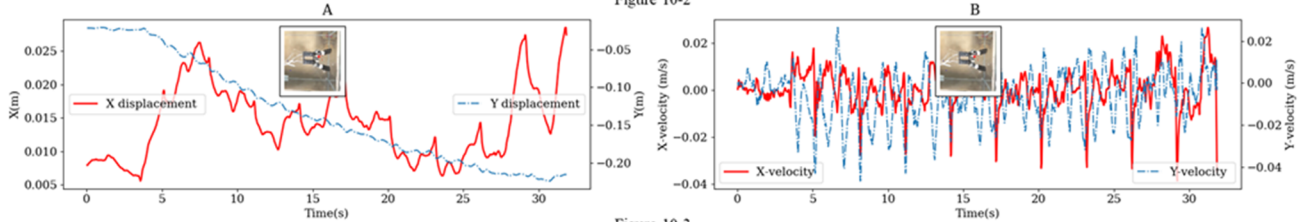


Figure 10-3

**Figure 10.** -1: The displacements and velocities along x and y axes for crawling locomotion. Note that there are two Y labels for each sub-figure and they have different scales. -2: The displacements(A-1, A-2) and velocities(B-1, B-2) along x and y axes, the rotation parameters(C-1, C-2) for turning-left (A) and turning-right (B) locomotion. Note that there are two Y labels for each sub-figure and they have different scales. -3: The displacements(A) and velocities(B) along x(vertical direction) and y(horizontal direction) axes for swimming locomotion. Note that there are two Y labels for each sub-figure and they have different scales.